Identifying Defects in Nanoscale Materials

Masa Ishigami,[1,2] Hyoung Joon Choi,[1,3] Shaul Aloni,[1,2] Steven G. Louie,[1,2] Marvin L. Cohen,[1,2] and A. Zettl[1,2,*]

[1]*Department of Physics, University of California at Berkeley, Berkeley, California 94720, USA*
[2]*Materials Sciences Division, Lawrence Berkeley National Laboratory, Berkeley, California 94720, USA*
[3]*Korea Institute for Advanced Study, 207-43 Cheongryangri Dongdaemun, Seoul 130-722, Korea*

(Received 28 April 2004; published 4 November 2004)

We have developed a novel iterative experimental-theoretical technique which can identify the atomic structure of defects in many-atom nanoscale materials from scanning tunneling microscopy and spectroscopy data. A given model for a defect structure is iteratively improved until calculated microscopy and spectroscopy data based on the model converge on the experimental results. We use the technique to identify a defect responsible for the electronic properties of a carbon nanotube intramolecular junction. Our technique can be extended for analysis of defect structures in nanoscale materials in general.

DOI: 10.1103/PhysRevLett.93.196803 PACS numbers: 73.22.–f

Nanoscale materials [1,2] have unique physical properties radically different from their bulk and extended solid equivalents. By tuning their structure, elemental composition, and size scale, a multitude of novel and useful properties can be obtained [3]. Particularly, because of the limited size scale of nanoscale materials, atomic scale defects are one of the most influential factors in determining their physical properties [4]. Thus, studying defects is important to enhancing the utility of these materials.

However, imaging techniques are limited at the atomic size scale, and the lack of proper analytical methods greatly hinders investigations of defects. Scanning electron microscopy cannot generally achieve sufficient resolution. Transmission electron microscopy can resolve atomic scale features but its resolution is limited for low mass elements [5,6]. Atomic scale resolution can readily be achieved using scanning tunneling microscopy (STM), but in any given STM image, local electronic densities of states and atomic structures are meshed together [7–12]. It is possible [13–16] to decipher the STM images of surface defects by calculating theoretical STM images and tunneling spectra of proposed models for the defects and comparing these to the experimental data. We have developed a novel iterative process which enables previously developed techniques to be reliable extended to complex systems involving a large number of atoms. In our process, a working model of the defects is systematically and iteratively improved until a match is obtained between the theoretical and the experimental data. In this Letter we apply our technique to identify the atomic structure of the most dominant defect in a carbon nanotube intramolecular junction.

Defects on carbon nanotubes are technologically important [17]. Single-wall carbon nanotubes, which are typically 1 nm in diameter, can be metallic or semiconducting depending on their helicity [17–19]. Individual nanotubes can be electrically contacted to yield functional nanoscale devices [20,21] useful for applications such as gas sensing [22,23]. It has been predicted [24] that even smaller electronic devices can be fabricated by joining nanotubes of different helicity. Such junctions can be formed by an insertion of topological defects into an otherwise perfect hexagonal bond network. The simplest and most elegant topological defect is a pentagon-heptagon pair (5-7 pair) defect. Several studies of intramolecular junctions (IMJs) using STM [25–28] and electronic transport measurements [29] have been reported previously. However, so far, identification of the exact atomic structure responsible for electronic properties at IMJs has not been achieved. Our analysis reveals a 5-7 pair to be the most dominant defect at a particular nanotube junction.

We begin by performing thorough scanning tunneling microscopy and spectroscopy (STS) measurements on a nanotube intramolecular junction. Our experimental procedure as described in [30] is similar to previously reported STM and STS experiments on carbon nanotubes [26–28,31]. The experimental data are then used as converging parameters for our iterative procedure to derive the atomic structure at the junction.

Figure 1 displays a bird's-eye view of a three-dimensional rendering of a constant current STM image

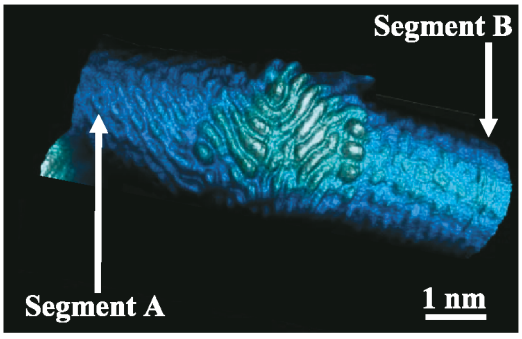

FIG. 1 (color). A bird's-eye view STM image of the nanotube junction acquired with $V_{\text{sample}} = +500$ mV and $I_{\text{tunnel}} = 0.20$ nA.

of a nanotube (which is not in a nanotube bundle) lying directly on the substrate. The junction located in the center of Fig. 1 joins two segments of the nanotube having different helicities. The periodicity of the features resolved suitably distant from the junction is consistent with a 4.26 Å periodicity of an electronic superstructure which is often observed on carbon nanotubes [32,33]. Using a procedure described in [31], tube indices are determined from our microscopy and spectroscopy data [34]. Segment A, which is located to the left of the junction, is best described by a (29, 5) index while segment B, located to the right of the junction, is consistent with (21, 3). Theoretically, nanotubes having these indices are metallic. In all subsequent relevant figures, segment A is to the left and segment B is to the right of the topographic images.

Spatially resolved tunneling spectra shown in Fig. 2(b), acquired at various locations indicated in Fig. 2(a), reveal a junction-localized electronic state centered approximately at +400 mV in the unoccupied states. The tunneling spectra acquired away from the junction show van Hove singularities (vHSs) expected for pristine nanotubes indicated by arrows in the figure. For segment A, vHSs are located at +442 and −429 mV, while for segment B they are at +481 and −770 mV. The spectrum at point 1 differs from the intrinsic spectrum for segment A. Unlike the intrinsic spectrum of segment A, there are no strong features in occupied states (negative V_{sample}), and the electronic density of states at +500 mV in the unoccupied states is close to zero. Thus, the feature appearing centered on +400 mV in the unoccupied states is the manifestation of the localized electronic state at the junction which coincidentally exists at a similar energy level as the intrinsic unoccupied state vHS of segment A. This electronic state has a broad energy full width of approximately 200 mV. The feature due to the localized electronic state weakens in strength near segment B, as shown in the spectra acquired at points 4 and 5. The intrinsic vHSs of segment B become apparent in the spectra acquired far away from the junction region.

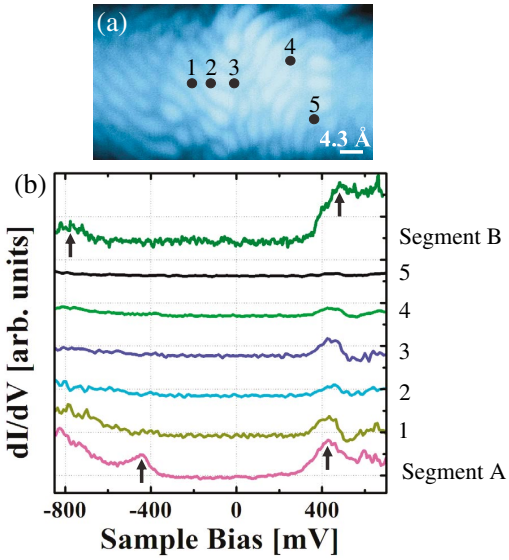

FIG. 2 (color). (a) An STM topography image acquired with $V_{\text{sample}} = +500$ mV and $I_{\text{tunnel}} = 0.20$ nA. The numbered points on the image indicate where dI/dV spectra in (b) are acquired. Segment A is to the left and segment B is to the right of the image. (b) Comparison of spatially resolved spectra on the junction at points 1 through 5 in (a), and spectra acquired on segment A and segment B acquired approximately 5 nm away from the junction. Arrows indicate the locations of van Hove singularities.

Bias dependent topography images of the junction are shown in Figs. 3(a) and 3(b). In these figures, whiter areas indicate regions with higher integrated density of electronic states [35]. Because the localized electronic state exists at +400 mV with a full width of 200 mV, if we compare STM images acquired with a sample bias voltage of +300 mV to one obtained with a +500 mV sample bias, the spatial extent of the state should be revealed. At +500 mV sample bias, as shown in Fig. 3(a), a complex wave pattern is observed over the junction with periodicities varying from 1.6 to 3.7 Å depending on direction and location. When the sample bias is lowered to +300 mV, as shown in Fig. 3(b), the wave pattern disappears. The complex wave pattern, which appears in Figs. 1 and 3(a), indicates the spatial distribution of the localized electronic state.

Although the energies and the spatial extent of the localized electronic state can be determined from the experimental data shown in Figs. 1–3, these data by themselves are not sufficient to determine the local atomic defect structure of the junction [26]. In order to

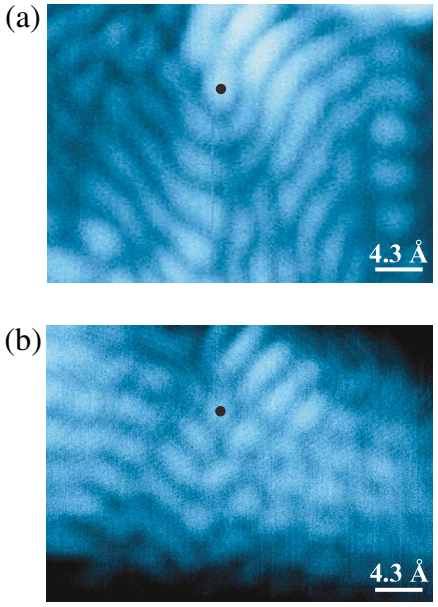

FIG. 3 (color). Detailed topographic images of the junction acquired with (a) $V_{\text{sample}} = +500$ mV and $I_{\text{tunnel}} = 0.20$ nA and (b) $V_{\text{sample}} = +300$ mV and $I_{\text{tunnel}} = 0.20$ nA. Black dots on (a) and (b) indicate the same location on the junction.

determine the defect structure responsible for the junction, we begin by building model junctions containing multiple 5-7 pair defects joining nanotube segments with experimentally determined chiral indices. These models must reproduce the observed geometry of the junction, such as the junction angle and corrugation observed at the junction. For example, in this specific junction, since a large corrugation is not observed, 5-7 pair defects on the top side (the side of the nanotube visible to STM imaging) must have the pentagon and the heptagon adjacent to each other. After this initial model building process, we subject the candidates to theoretical calculations to obtain both local density of states (LDOS) in the junction region and theoretical STM topography images. While compensating to keep the junction angle and corrugation consistent with the experiment, adjustments to the models are made until a match to the experimental data is obtained. Our analysis yields a model, shown in Fig. 4, containing two 5-7 pairs. One 5-7 pair is on the top side of the tube and is responsible for the electronic properties observed in the experiment. The other 5-7 pair, necessary to reproduce the junction angle, is on the other side of the nanotube and is "hidden" from the STM imaging. For this second pair, the pentagon and the heptagon do not lie next to each other. The second pair does not contribute significantly to the electronic properties on the top side of the junction. For the theoretical calculations we use a one-electron tight-binding method with a nearest neighbor hopping energy of -2.66 eV. Green's function is calculated using a numerical generalization of a previously developed formalism [36]. The on site energy in the $(21, 3)$ nanotube is lowered by 140 mV to mimic the observed locations of the vHSs of the nanotubes.

With the help of the constructed model, we identify the center of the wave pattern seen in Fig. 1 to be a 5-7 pair defect. Figure 5(b) shows theoretical LDOS spectra at six atomic sites of a particular hexagon highlighted on the wire frame picture of our model junction. The hexagon is chosen because it is spatially close to where the experimental spectra are acquired and to show the typical local variation of the LDOS spectra in the junction region. The calculated LDOS spectra show localized features at the junction only between $+300$ and $+500$ mV in the unoccupied states. At the representative hexagon in Fig. 5(a) there are features near $+400$ mV at carbon atoms 1 and 3, and between $+350$ and $+500$ mV at the other sites, as shown in Fig. 5(b). In reality, the STM tip samples more than one atomic site and we anticipate the tip to average out these features. The experimentally observed energy width of the localized state [Fig. 2(b)] is consistent with our calculations. In the occupied states, no junction-specific features appear in the model in agreement with the experiment. In addition, using the LDOS calculations, we have computed theoretical STM images at various sample bias voltages using a method previously developed by others [37]. As shown in Fig. 6(a), at a sample bias voltage of $+500$ mV, a wave pattern appears at the junction near the 5-7 pair with periodicities of 2.1 and 3.7 Å, in agreement with the STM topography measurements. Figure 6(b) shows that the wave pattern disappears for a $+300$ mV sample bias, again in agreement with the experiment. Our model junction has properties equivalent to the measured properties particularly near the black dots in Figs. 3(a) and 3(b). Hence, there is a 5-7 pair defect at the location indicated by the black dot, and the defect is the dominant contributor to the electronic properties of the junction.

Our technique relies on STM or STS, which can achieve atomic scale resolution on many nanoscale materials deposited or assembled on conductive substrates [1]. The theoretical part of the technique is also not specific to carbon nanotubes but is applicable to many nanoscale materials. Thus, our integrated experimental and/or theoretical technique can be used to investigate how defects influence physical properties of nanoscale

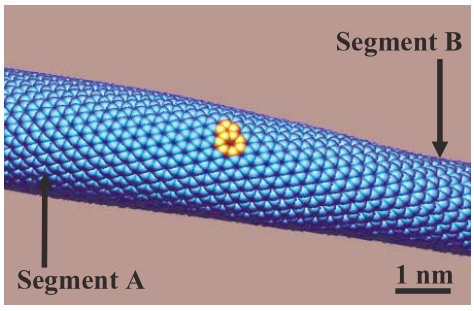

FIG. 4 (color). Theoretical model of the junction. There are two pentagon-heptagon pair defects in the model. One is visible and highlighted in the figure. The other pair is on the hidden side of the tube and is not accessible by the experiment.

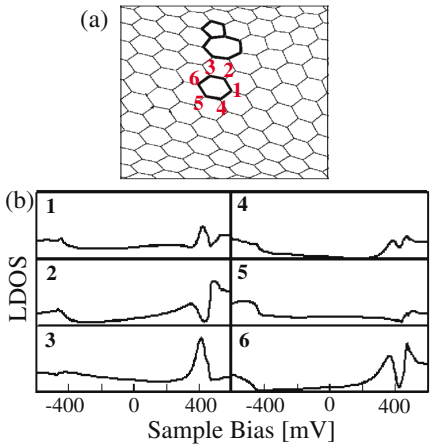

FIG. 5 (color). (a) A wire frame model of the junction near the visible 5-7 pair defect. Numbers on a highlighted hexagon indicate atomic sites where local electronic densities of states shown in (b) are calculated. Segment A is to the left and segment B is to the right of the wire frame model. (b) The local densities of states at atomic sites on the highlighted hexagon in (a).

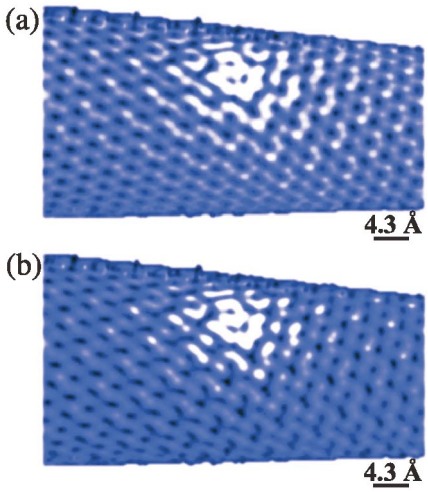

FIG. 6 (color). Calculated STM images for (a) $V_{\text{sample}} = +500\,\text{mV}$ and (b) $V_{\text{sample}} = +300$ mV.

materials in general. We anticipate that the technique can be used to explore problems such as the exciton lifetimes in quantum dots [38], influence of defects on transport [39], and mechanical properties [4] of nanotubes, nanowires, and nanocrystals.

This work was supported in part by the National Science Foundation under Grants No. DMR-9301738, No. DMR-9501156, and No. DMR00-87088 and by the Director, Office of Energy Research, Office of Basic Energy Sciences, Division of Materials Sciences of the U.S. Department of Energy under Contract No. DE-AC03-76SF00098 within the sp^2 Nanomaterials Program. M. I. acknowledges the support of the Hertz Foundation.

*Electronic address: azettl@socrates.berkeley.edu

[1] F. Rosei, J. Phys. Condens. Matter **16**, S1373 (2004).
[2] P. Moriarty, Rep. Prog. Phys. **64**, 297 (2001).
[3] A. P. Alivisatos, Science **271**, 933 (1996).
[4] E. Z. da Silva, A. J. R. da Silva, and A. Fazzio, Phys. Rev. Lett. **87**, 256102 (2001).
[5] B. Fultz and J. M. Howe, *Transmission Electron Microscopy and Diffractometry of Materials* (Springer-Verlag, New York, 2001).
[6] J. C. H. Spence, Mater. Sci. Eng., R **26**, 1 (1999).
[7] J. A. Stroscio and W. J. Kaiser, *Scanning Tunnelling Microscopy* (Academic, San Diego, 1993).
[8] R. Wiesendanger, *Scanning Probe Microscopy and Spectroscopy* (Cambridge University, Cambridge, England, 1994).
[9] F. Besenbacher, Rep. Prog. Phys. **59**, 1737 (1996).
[10] H. Neddermeyer, Rep. Prog. Phys. **59**, 701 (1996).
[11] G. Binnig and H. Rohrer, Rev. Mod. Phys. **71**, S324 (1999).
[12] A. Yazdani and C. M. Lieber, Nature (London) **401**, 227 (1999).
[13] R. J. Hamers and U. K. Kohler, J. Vac. Sci. Technol. A **7**, 2854 (1989).
[14] R. Schaub *et al.*, Phys. Rev. Lett. **87**, 266104 (2001).
[15] S. Okano and A. Oshiyama, Surf. Sci. **554**, 272 (2004).
[16] A. V. Krasheninnikov *et al.*, Phys. Rev. B **63**, 245405 (2001).
[17] M. S. Dresselhaus, G. Dresselhaus, and P. Avouris, *Carbon Nanotubes: Synthesis, Structure, Properties, and Application* (Springer-Verlag, New York, 2001).
[18] J. W. G. Wildoer, L. C. Venema, A. G. Rinzler, R. E. Smalley, and C. Dekker, Nature (London) **391**, 59 (1998).
[19] T. W. Odom, J.-L. Huang, P. Kim, and C. M. Lieber, Nature (London) **391**, 62 (1998).
[20] M. Bockrath, D. H. Cobden, P. L. McEuen, N. G. Chopra, A. Zettl, A. Thess, and R. E. Smalley, Science **275**, 1922 (1997).
[21] S. J. Tans *et al.*, Nature (London) **386**, 474 (1997).
[22] P. G. Collins, K. Bradley, M. Ishigami, and A. Zettl, Science **287**, 1801 (2000).
[23] J. Kong *et al.*, Science **287**, 622 (2000).
[24] L. Chico *et al.*, Phys. Rev. Lett. **76**, 971 (1996).
[25] P. G. Collins *et al.*, Science **278**, 100 (1997).
[26] M. Ouyang, J.-L. Huang, C. L. Cheung, and C. M. Lieber, Science **291**, 97 (2001).
[27] M. Ouyang, J.-L. Huang, and C. M. Lieber, Phys. Rev. Lett. **88**, 066804 (2002).
[28] H. Kim *et al.*, Phys. Rev. Lett. **90**, 216107 (2003).
[29] Z. Yao, H. W. C. Postma, L. Balents, and C. Dekker, Nature (London) **402**, 273 (1999).
[30] Purified carbon nanotubes grown by laser ablation were used for this study; the nanotubes were purchased from Tubes@Rice. Nanotubes are first annealed in air at 400 °C for 1 h and subsequently in vacuum at 600 °C for 2 h to clean their surfaces. The treated nanotubes are deposited on a Au(111) substrate from a 1,2-dichloroethane suspension. The samples are outgassed at 250 to 400 °C for over 2 h in ultrahigh vacuum prior to STM experiments. A homemade scanning tunneling microscope operated at 77 K is used for the experiments.
[31] L. C. Venema, V. Menueir, P. Lambin, and C. Dekker, Phys. Rev. B **61**, 2991 (2000).
[32] W. Clauss *et al.*, Europhys. Lett. **47**, 601 (1999).
[33] C. L. Kane and E. J. Mele, Phys. Rev. B **59**, R12 759 (1999).
[34] Segment A has a chiral angle of $7.8 \pm 2.0°$, while segment B has a chiral angle of $7.1 \pm 1.0°$ both from the zigzag direction. Tunneling spectroscopy measurements reveal the separation of first van Hove singularities (vHSs) in these segments to be 871.57 and 1251.81 mV, respectively. From height measurements and from the positions of vHSs, we deduce that these are metallic nanotube segments with diameters of 26.1 ± 1.9 Å and 18.6 ± 1.4 Å, respectively.
[35] J. Tersoff and D. R. Hamann, Phys. Rev. Lett. **50**, 1998 (1983).
[36] H. J. Choi and J. Ihm, Solid State Commun. **111**, 385 (1999).
[37] V. Meunier and P. Lambin, Phys. Rev. Lett. **81**, 5588 (1998).
[38] D. F. Schroeter, D. J. Griffiths, and P. C. Sercel, Phys. Rev. B **54**, 1486 (1996).
[39] A. Calzolari, N. Marzari, I. Souza, and M. B. Nardelli, Phys. Rev. B **69**, 35108 (2004).